J. Fluid Mech. (1982), *vol.* 123, *pp.* 399–423
Printed in Great Britain

Measurements and predictions of fully developed turbulent flow in a simulated rod bundle

By W. J. SEALE

School of Mechanical Engineering, University of Bradford, Richmond Road, Bradford BD7 1DP, U.K.

(Received 29 October 1981)

Fully developed air flow has been investigated over a Reynolds-number range of 82800–346700 in a duct that simulates two interconnected subchannels of a rod bundle with a pitch/diameter ratio of 1·20. Based on equivalent hydraulic diameter, friction factors were found to be 2 % lower than for pipe flow. Detailed measurements were made at a Reynolds number of 200000 of axial velocities, secondary velocities, and the Reynolds stresses. The distribution of axial velocity near the walls (normalized with the local friction velocity) could be expressed by an inner law of the wall for y_+ up to 1500. Distributions of the normal Reynolds stresses and the mean turbulence kinetic energy were similar to those observed in a number of pipe and two-dimensional channel flows and could be correlated using the axial-velocity fluctuations normalized with the local friction velocity. Maximum secondary velocities were about 1·5 % of the bulk axial velocity. The 'k–ϵ' turbulence model and an algebraic vorticity source for generating secondary velocities enabled the computation of axial velocities, secondary velocities, and mean turbulence kinetic energies that are in satisfactory agreement with those measured.

1. Introduction

Over the past 15 years a number of turbulence models and numerical procedures have been developed that allow turbulent flow to be predicted in ducts of non-circular cross-section. Much of this work has been done to permit the calculation of flow and heat transfer in the core of a nuclear reactor, where the fuel elements are arranged as a matrix of rods along which the coolant flows axially.

The most widely used procedure has been based on the 'k–l' (or 'k–ϵ') turbulence model for the effective viscosity, together with a model for the normal Reynolds stresses that allows the small but significant secondary velocities to be generated. These procedures have been used to predict distributions of mean axial velocity, turbulence kinetic energy, and secondary velocities in rod-bundle geometries by a number of investigators (Carajilescov & Todreas 1976; Aly, Trupp & Gerrard 1978; Seale 1979; Trupp & Aly 1979; Bartziz & Todreas 1979; Gosman & Rapley 1980). However, the results of these applications have often proved inadequate and contradictory (Seale 1982), and the lack of high-quality experimental measurements of the turbulence structure in rod bundles has inhibited the development of the turbulence models.

Turbulent diffusion between adjacent subchannels in rod-bundle flow is also known to be much higher than predicted by simple isotropic diffusion theory and is relatively insensitive to changes in gap width. A variety of explanations have been suggested to explain this behaviour. For example Rehme (1978) found that the effective

diffusivity in a rod bundle is highly anisotropic, with very large apparent diffusivities parallel to the rod surface and through the gaps. On the other hand Nijsing & Eifler (1970) have claimed that the unexpected behaviour of the diffusion can be entirely explained by the presence of secondary flows. Seale (1979) supported Rehme and indicated high anisotropies as the primary source of high intersubchannel mixing, with secondary flows having only a small effect.

Secondary flows, although producing significant and observable modifications to the mean flow, are extremely small and no reliable measurements have been reported in rod bundles. A complicating feature is that it is extremely difficult to build a rod bundle with the precision necessary to ensure that cross-flows caused by the geometric imperfections do not swamp those generated by the turbulence structure.

The object of the present work was to build a simulated rod bundle to an extremely high geometric precision and to measure with as much accuracy as possible the primary quantities which it is claimed can be predicted by turbulence modelling, i.e. axial velocity, turbulence kinetic energy, and the secondary velocities.

Previous experimental investigations of the Reynolds stresses and secondary velocities in fully developed flow in rod bundles have been reported by Kacker (1973), Rowe, Johnson & Knudsen (1974), Kjellström (1974), Trupp & Azad (1975), Carajilescov & Todreas (1976), Rehme (1978), Aly *et al.* (1978) and Hooper (1980).

The turbulence structure for fully developed flow through the subchannels formed by the rod array depends on the pitch-to-diameter ratio p/d. For fairly open ducts ($p/d \geqslant 1{\cdot}2$) the distributions of the three components of the normalized turbulence intensity normal to a wall are similar to those measured in circular ducts or between plane surfaces. For more closely spaced arrays the turbulence structure, especially in the rod-gap region, departs markedly from the pipe-flow distributions. This behaviour is generally attributed to the increasing strength of secondary flows as the rod-gap spacing is reduced. However, most attempts to measure the tiny secondary velocities in rod bundles have not been successful.

Kacker (1973), using a hot-wire technique suggested by Hoagland (1960), measured secondary flows in a circular duct containing two small rods. In the gap between the rods the secondary velocities were about 0·5 % of the mean velocity.

Rowe *et al.* (1974), using a laser-Doppler anemometer, measured axial turbulence intensities in ducts containing rods arranged in a square array ($p/d = 1{\cdot}25$ and $1{\cdot}125$). In the gap region high values of axial intensity were observed, which became more energetic as the rod gap was decreased. The presence of secondary flows were inferred from distortions of the intensity distribution.

Kjellström (1974) used a rotatable hot wire to measure the secondary flows in a triangular-array rod bundle ($p/d = 1{\cdot}217$), but the results were not satisfactory and there appeared to be a large-scale circulation in the entire bundle with a circulation velocity about 1 % of the bulk velocity. This circulation was ascribed to small geometric inaccuracies in the tunnel. Trupp & Azad (1975) were unable to measure the secondary velocities using X-array probes in triangular-array rod bundles and also reported problems due to geometric imperfections.

Carajilescov & Todreas (1976) used a laser-Doppler anemometer in a duct simulating an interior subchannel of a triangular array ($p/d = 1{\cdot}123$) but experimental error precluded identification of secondary velocities having a magnitude less than 0·67 % of bulk axial velocity.

Rehme (1978) investigated turbulent flow in a duct consisting of a single row of rods ($p/d = 1{\cdot}071$) between two flat walls. The rotated hot-wire technique was used to measure the Reynolds stresses. Secondary flows were evident from the distortions

to the distributions of the turbulence intensities but again they could not be measured.

Aly *et al.* (1978) investigated turbulent flow in an equilateral triangular duct, regarded as representative of rods on a triangular array having unit pitch-to-diameter ratio (i.e. rods touching). Reynolds stresses and secondary velocities were measured using an X-array probe and checked using a rotatable 45° slant wire. The distributions of turbulence intensities normal to the walls were similar to those observed in pipe flows, maximum secondary velocities were about 1·5% of the bulk velocity.

Hooper (1980) used hot-wire anemometry to measure the Reynolds stresses in two ducts simulating rods on a square array ($p/d = 1{\cdot}194$, $1{\cdot}107$). Differences in the turbulent flow structure from that of axisymmetric pipe flow were found; these departures were strongly dependent on pitch-to-diameter ratio. This behaviour was attributed to secondary flows, although these could not be resolved by direct measurement.

In the present work on the subchannel of a simulated rod bundle, measurements have been made of the axial pressure gradient, local wall shear stress, mean axial velocities, the two in-plane secondary velocities, and distributions of the five Reynolds stresses (excluding the extremely small in-plane shear stress $-\overline{\rho vw}$). The measurements were made at a single Reynolds number of 200000 since most of the quantities are only weak functions of Reynolds number and the primary aim of the research was to produce accurate data for use in testing prediction methods.

From an assessment of likely construction tolerances it was clear that a long rod bundle having the necessary geometric precision could not be built. Disturbances to the flow caused by the support structure that holds the rods in position are also very difficult to avoid. It was felt that for the purpose of comparison with prediction methods the major features of the turbulence structure and the secondary flows would be observed in a duct that simulated typical subchannels of a rod bundle. A prediction method that cannot at least reproduce the flow in an ideal simulated subchannel is unlikely to be satisfactory when applied to the subchannels of an 'infinite' rod bundle.

A simple shape was chosen: two half rods set in a rectangular-section duct. The interconnected subchannels that this forms are a primary feature of the subchannels in all rod bundles, and the duct shape lends itself to accurate location over the full length of the tunnel. The interior corners of the duct generate distinct patterns of secondary flows: these would not be present in the subchannels of a rod bundle. However, corner flows have been widely investigated, and their presence in the present duct was regarded as a known standard against which the measured secondary velocities in the core and gap regions of the subchannel could be compared.

The Reynolds stresses and secondary velocities were measured using the rotated hot-wire technique. This method requires six separate measurements to be made at a given position: measurements were therefore confined to a limited number of points.

Attempts were made to reproduce the measured distributions of axial velocity, secondary velocity, and mean turbulence kinetic energy by numerical prediction of the flow. The predictions were based on the general elliptic finite-difference procedure of Gosman *et al.* (1969) and on the 'k–ϵ' turbulence model (Launder & Spalding 1974). A novel algebraic expression was derived for the source of axial vorticity to allow a correct pattern of secondary velocities to be generated and to give agreement with the experimental data.

2. Prediction of the turbulent flow

Use of the 'k–ϵ' turbulence model and the Gosman numerical integration scheme is a well-established technique and only a brief outline of it will be given here.

Consider the turbulent flow along a straight duct of non-circular cross-section. For ease of interpretation the equations of motion will be written in Cartesian coordinates with x along the main duct axis, y normal to, and z parallel to a wall. The axial velocity is U, and V and W are the in-plane secondary velocities. The corresponding fluctuating components of the velocities are u, v and w, and an overbar designates time averaging.

2.1. *Axial-momentum equation*

The following equation describes the conservation of axial momentum for fully developed turbulent flow of a constant-property fluid:

$$\rho\left(V\frac{\partial U}{\partial y}+W\frac{\partial U}{\partial z}\right)=-\frac{\partial P}{\partial x}+\mu\left(\frac{\partial^2 U}{\partial y^2}+\frac{\partial^2 U}{\partial z^2}\right)-\rho\left(\frac{\partial\overline{uv}}{\partial y}+\frac{\partial\overline{uw}}{\partial z}\right). \tag{1}$$

The turbulence shear stresses were simulated using the concept of an eddy viscosity (assumed to be locally isotropic); the eddy viscosity was calculated from the 'k–ϵ' turbulence model, viz.

$$\mu_t = C_\mu \rho k^2/\epsilon, \tag{2}$$

where C_μ is a constant, π is the density, k is the mean turbulence kinetic energy, and ϵ is the dissipation of the turbulence kinetic energy. Both k and ϵ were found from the solution of the appropriate conservation equations.

2.2. *Secondary velocities*

The calculation of the secondary velocities V and W was performed according to the scheme proposed by Gosman *et al.* (1969) in which the equations describing the conservation of momentum in the y- and z-directions are replaced by a stream function ψ and the axial vorticity ω (thus eliminating the in-plane pressure gradients), i.e.

$$\rho V=-\frac{\partial\psi}{\partial z},\quad \rho W=\frac{\partial\psi}{\partial y},\quad \omega=\frac{\partial V}{\partial z}-\frac{\partial W}{\partial y}.$$

The equation for the conservation of axial vorticity becomes

$$\frac{\partial}{\partial y}\left(\omega\frac{\partial\psi}{\partial z}\right)-\frac{\partial}{\partial z}\left(\omega\frac{\partial\psi}{\partial y}\right)-\frac{\partial}{\partial y}\left(\frac{\partial(\mu\omega)}{\partial y}\right)-\frac{\partial}{\partial z}\left(\frac{\partial(\mu\omega)}{\partial z}\right)+S_\omega=0, \tag{3}$$

where the vorticity-production term S_ω is given by

$$S_\omega=-\rho\frac{\partial^2}{\partial y\,\partial z}(\overline{v^2}-\overline{w^2})+\rho\left(\frac{\partial^2\overline{vw}}{\partial y^2}-\frac{\partial^2\overline{vw}}{\partial z^2}\right). \tag{4}$$

This term can be regarded as the source of the secondary flows.

A number of investigators have shown that the shear stress terms in (4) are negligibly small compared with the normal-stress terms; see for example the measurements of Brundrett & Baines (1964) in a square duct, and those of Aly *et al.* (1978) in a triangular duct (although deep in the corner of the latter duct there was a significant contribution from the shear stresses). Trupp & Aly (1979) performed calculations with and without the shear-stress terms for the subchannels of a rod bundle and found that the normal-stress vorticity production predominated everywhere in the flow cell.

Vorticity production was therefore considered to be solely due to the imbalance in the normal stresses, and (4) becomes

$$S_\omega = -\rho \frac{\partial^2}{\partial y\, \partial z}(\overline{v^2} - \overline{w^2}). \tag{5}$$

In the computations reported here, this term has been evaluated in local coordinates aligned with the nearest wall since the justification for omitting the shear stresses rests on empirical evidence in which the axes were normal and parallel to a wall.

For the present case of weak secondary flows and use of an eddy viscosity Launder & Ying (1973) reduced the differential transport equations for the Reynolds stresses proposed by Hanjalic & Launder (1972) and derived the following algebraic equation for the difference in the normal stresses:

$$\bar{v}^2 - \bar{w}^2 = -\frac{Ck}{\rho\epsilon}\mu_t\left(\left(\frac{\partial U}{\partial y}\right)^2 - \left(\frac{\partial U}{\partial z}\right)^2\right), \tag{6}$$

where C is a constant. When this equation was used, together with (5), to generate the axial vorticity in the present duct the pattern of secondary flows produced did not allow the measured distributions of axial velocity and turbulence kinetic energy to be reproduced. After a careful examination of the problem the following algebraic equation, which gives the source of axial vorticity directly, was derived:

$$S_\omega = 0{\cdot}864 \frac{\bar{\tau}}{(\hat{y}^2_{\max})^2} Y_P\, Y_L\, Y_N \frac{d\hat{y}}{dz}, \tag{7}$$

where $\bar{\tau}$ = mean wall shear stress, y = normal distance from wall, $\hat{y}$ = normal distance from wall to surface of no shear, $\hat{y}_{\max}$ = maximum value of $\hat{y}$, $d\hat{y}/dz$ = rate of change of $\hat{y}$ parallel to wall, and

$$Y_P = 1 - \hat{y}/\hat{y}_{\max}, \quad Y_M = 1 - 2{\cdot}4\, Y_P^2, \quad Y_L = 1 - y/\hat{y}_{\max},$$

$$Y_N = \{1 + Y_M + (4 - Y_M)\, Y_L^2\} - \{(1 - Y_L^2)(4 - Y_M)\}.$$

The surface of no shear is assumed to be coincident with the position of the maximum axial velocity on the normal from the wall. A full derivation of (7) has been given by Seale (1982): for convenience this is summarized in appendix A.

2.3. *Solution of the equations*

The differential transport equations for stream function, vorticity, dissipation of turbulence kinetic energy, turbulence kinetic energy and axial velocity can all be expressed in a common elliptic form (Seale 1979):

$$a\left(\frac{\partial}{\partial y}\left(\phi \frac{\partial \psi}{\partial z}\right) - \frac{\partial}{\partial z}\left(\phi \frac{\partial \psi}{\partial y}\right)\right) - \frac{\partial}{\partial y}\left(b_1 \frac{\partial}{\partial y}(c\phi)\right) - \frac{\partial}{\partial z}\left(b_2 \frac{\partial}{\partial z}(c\phi)\right) + d = 0, \tag{8}$$

where ϕ is taken as the dependent variable and the functions a, b_1, b_2, c and d for each equation are given in table 1. The values of the various constants were those recommended by Launder & Spalding (1974):

$$C_{\epsilon 1} = 1{\cdot}44, \quad C_{\epsilon 2} = 1{\cdot}92, \quad C_\mu = 0{\cdot}09, \quad Pr_\epsilon = 1{\cdot}3 \quad \text{and} \quad Pr_k = 1{\cdot}0.$$

The equations were solved for an irregular Cartesian grid using an upwind finite-difference technique based on the general elliptic procedure of Gosman *et al.* (1969). Where the grid met curved surfaces, special treatment was required for the representation of the boundary condition for axial velocity, and a simple algebraic expression was derived which gave the correct momentum flow to the surface. The

ϕ	a	$b_1\ (=b_2)$	c	α
ω	1	1	μ	$-\rho\dfrac{\partial^2}{\partial y\,\partial z}(\overline{v^2}-\overline{w^2})$
ψ	0	$1/\rho$	1	$-\omega$
ϵ	1	$\dfrac{\mu+\mu_T}{Pr_\epsilon}$	1	$-C_{\epsilon 1}\dfrac{\epsilon}{k}\mu_t\left(\left(\dfrac{\partial U}{\partial y}\right)^2+\left(\dfrac{\partial U}{\partial z}\right)^2\right)+\rho C_{\epsilon 2}\dfrac{\epsilon^2}{k}$
k	1	$\dfrac{\mu+\mu_t}{Pr_k}$	1	$-\mu_t\left(\left(\dfrac{\partial U}{\partial y}\right)^2+\left(\dfrac{\partial U}{\partial z}\right)^2\right)+\rho\epsilon$
U	1	$\mu+\mu_t$	1	$\partial P/\partial x$

TABLE 1. Coefficients in the elliptic differential equations for ω, ψ, ϵ, k and U

remaining boundary conditions presented no special problems at curved surfaces. Details of the boundary conditions are given in Seale (1979). However, the explicit form of the logarithmic law due to Patankar & Spalding (1970) used for deriving the boundary condition for axial velocity, was modified slightly to give agreement with the measured distributions of velocity near the walls.

The majority of computations were performed with a 21×25 grid over a symmetrical quadrant of the duct. A few comparative solutions were obtained at a single Reynolds number with a 60×70 grid: agreement was within 1 % for friction factors and 5 % for the secondary velocities.

3. Wind tunnel and instrumentation

3.1. *Wind tunnel*

The wind tunnel, up to the test section of the current work, was that used previously by Seale (1977) and is fully described there. Atmospheric air was blown through the tunnel and discharged to atmosphere at the exit.

Following the blower, the air passed through an air cooler, which allowed precise control of the air temperature, through a flow-measuring orifice (to BS1042) and into a large transition box equipped with baffles and screens. The air was discharged from the transition box through a contraction having a rectangular exit, into a duct of rectangular cross-section 9 m long followed by a gentle contraction 1·8 m long into the test section. The velocity distribution of the air entering the working section of the tunnel was symmetrical to within 1 %.

The length of the test section of the tunnel was 18 m, i.e. 120 equivalent diameters.

3.2. *Test section*

The cross-section of the tunnel is shown in figure 1. The tunnel, which simulates two adjacent subchannels of a rod bundle and had no support structure to disturb the air flow, was made from precision-machined Perspex rigidly held within a steel frame. Considerable care was taken to ensure the precise location of all parts of the tunnel. A detailed survey of the tunnel showed the following maximum deviations from the nominal dimensions: 0·6 mm over the first 9 m, 0·3 mm for the next 4 m, and 0·1 mm over the last 5 m. Distortion of the tunnel caused by the air pressure was less than 0·2 mm at entry.

The central axis of the tunnel was located to within 100 μm over the 18 m length using a surveyor's level.

Static pressure taps were positioned along the upper flat surface of the tunnel at 1·85 m axial intervals giving 10 tapping points. The test plane was located 120

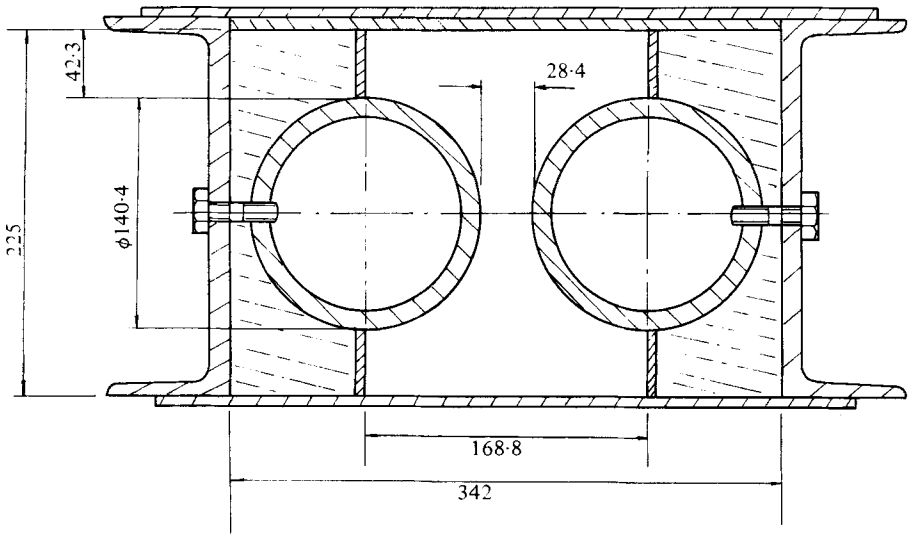

FIGURE 1. Cross-section of tunnel (dimensions in mm).

equivalent diameters from the test-section inlet, and 10 mm from the end of the duct. End effects at this position could not be detected.

3.3. *Measuring technique*

The determination of the Reynolds stresses and the secondary velocities at any point required separate measurements to be made using a Pitot tube, a normal hot-wire anemometer, and a 45° slant hot wire rotated into four angular positions. The technique employed by Rehme (1977) was used to achieve the extremely accurate positioning required by this procedure. A microscope is focused sharply onto the end of a pointer, the absolute position of which is known. The pointer is removed, and, without altering the setting of the microscope, the measuring probe is brought sharply into focus. The position of the probe is then known to within about 16 μm, the depth of field of the microscope. A DISA 55H01 traversing unit was used to locate the probe in the field of flow.

The angle between the mid-section of the slant wire and the central axis of the duct was set to within 0·1° of 45° using a comparator method.

3.4. *Instrumentation*

Axial velocities and wall shear stresses were measured by a Pitot tube with outside diameter 1·473 mm and inside-to-outside diameter ratio of 0·6. The Pitot pressure was measured with a Betz manometer (accuracy $\pm$0·05 mmH_2O).

Turbulence measurements were made using DISA constant-temperature hot-wire anemometers: the 55P12 single slant wire and the 55P11 single normal wire. These probes have a sensing length of 1·25 mm. The response of the wires was measured by a Solartron Microprocessor Digital Voltmeter 7055 and a DISA 55035 r.m.s. voltmeter.

3.5. *Calibration procedure*

All the hot-wire probes were calibrated external to the tunnel using the DISA 55090 calibration facility. Since the air temperature during the calibration differed by up to 3 °C from that of the measurements in the tunnel, an adjustment was made to the calibration results. The adjustment was determined using the procedure of Bearman

(1971). This technique was checked experimentally over a temperature range of 30 K and found to be accurate to better than 1 %.

The calibration was expressed in the form $E^2 = E_0^2 + BU^n$, where U is the known velocity of the air, E is the d.c. voltage across the anemometer, and E_0^2, B and n were regarded as calibration constants. These were found by using a NAG optimization routine†, which minimizes the sum of the squares of the differences between the experimental points and the calibration curve. This gave a typical maximum deviation between the measured points and the fitted calibration curve of 0·017 % on voltage and 0·11 % on velocity.

The hot-wire anemometers were calibrated before and after each traverse: the results obtained during the traverse were only accepted if for any voltage E the velocities given by the two calibrations did not differ by more than 1 % and the term $(E^2 - E_0^2)^{1/n}$ did not change by more than 0·25 %. The reasons for these criteria are given in appendix B.

4. Experimental results and discussion

4.1. *General*

Before starting the programme of tests, measurements were made at the tunnel exit to confirm that the flow was symmetric between the four quadrants. The axial velocity distribution was measured along the central vertical axis of the tunnel and along horizontal traverses midway between the flat surface and the tubes. Symmetry of the wall shear stress was checked at a limited number of positions along the upper and lower flat surfaces. The results showed that deviations from symmetry were within 0·3 % for the axial velocity and within 0·7 % for the wall shear stress.

On the central horizontal axis along the gap between the two subchannels the axial shear stress fell to zero. Similarly the Reynolds shear stress $-\rho\overline{uw}$ along the central vertical axis did not differ from zero by an amount greater than the uncertainty in measuring the Reynolds shear stresses (about $0{\cdot}02U_\tau^2$).

It is reasonable to conclude that the flow was symmetrical and that the results measured in the single quadrant were representative of the entire duct cross-section.

Since the six separate measurements at each point required several days of testing, the question was considered of whether identical conditions could be reproduced for each test. The temperature of the air could be controlled and was held constant. Variations in atmospheric pressure however affected the responses of the flow-measuring orifice, the Pitot tube, and the hot-wire anemometer. It was concluded that it was not possible to compensate fully for changes in barometric pressure, but, since the measurements of the Reynolds stresses and the secondary velocities were in terms of ratios, small changes in exit conditions would not affect the derived results. Accordingly, the pressure difference across the orifice monitoring the air flow entering the tunnel was held constant since this could be done relatively simply. The second-order effect of humidity change on air density was not considered.

4.2. *Tests performed*

Three sets of tests were performed on the tunnel.

(i) Measurements were made of the pressure gradient along the tunnel for a range of Reynolds numbers from 82800 to 346700.

† NAG FORTRAN Mark 7 Library (Routine E04JAF).

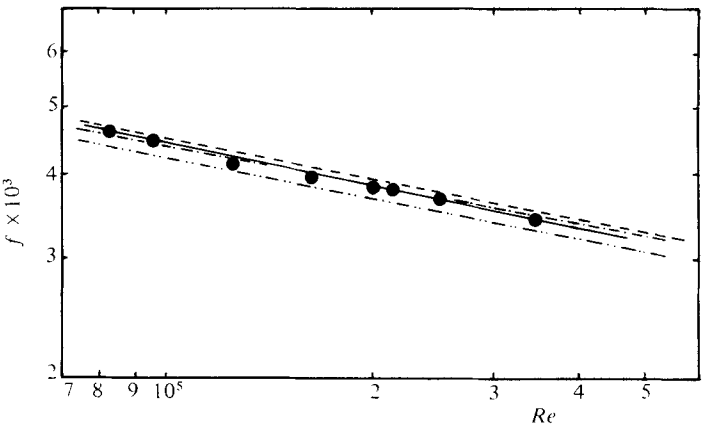

FIGURE 2. Friction factor versus Reynolds number in simulated rod bundle. ●, present experimental data; – · – · – · –, computed (with secondary flows); — · · — · · — · · —, computed (without secondary flows); ————, $f = 0{\cdot}0475Re^{-0{\cdot}206}$ (least-squares fit to the present experimental data); – – – – – – – –, Kármán–Nikuradse.

(ii) Measurements were made of axial velocities (using a Pitot tube) and wall shear stresses on a fine grid covering the test quadrant, at a Reynolds number of 200000.

(iii) Over a more restricted grid, measurements were made of axial velocities, secondary velocities, and Reynolds stresses at a Reynolds number of 200000. These were measured along vertical traverses perpendicular to the top flat surface 0, 15, 30, 45, 60 and 75 mm from the central vertical axis of the tunnel. Measurements were made at 5 mm intervals along these traverses, with extra points near the walls.

A number of these tests were repeated. No problems were met in re-establishing the conditions of a previous test and the results were always within the uncertainty of the measuring instrument.

4.3. *Friction factor*

The axial pressure gradient along the tunnel was derived from the 10 static pressure taps on the upper flat surface. A straight line could be drawn through zero at the tunnel exit and through the pressures of all but the first tapping point. The gradient of the line was found from a least-squares fit constrained to pass through zero at the tunnel exit.

The measured axial pressure gradient was corrected for the effect of the compressibility of the air by assuming the flow to be adiabatic. At the maximum Mach number of 0·17 the required correction was 4%.

The mass flow was measured by the orifice at tunnel entry. The friction factor f was computed from

$$f = \frac{-\frac{1}{4}D\,dP/dx}{\frac{1}{2}\rho U^2},$$

where D is the hydraulic diameter and U is the bulk mean velocity. The 95% confidence limit on the value of the friction factor is estimated to be within $\pm 2\%$, the main source of uncertainty being the measurement of the mass flow using an orifice.

The results are given in the form friction factor f versus Reynolds number Re in figure 2. A least-squares fit to the data gave the following expression:

$$f = 0{\cdot}0475Re^{-0{\cdot}206}.$$

The friction factors are about 2% lower than the values predicted by the Kármán–Nikuradse correlation† for friction factors in smooth circular tubes.

An estimate of the friction factor in the tunnel has been made using a method proposed by Malak, Hejna & Schmid (1975) in which the turbulent friction factor in a non-circular duct is derived from a knowledge of the laminar friction factor in the duct. (A similar method has been proposed by Rehme 1973). The laminar friction factor in the present duct, computed using the prediction procedure for turbulent flow but omitting all turbulence effects, was found to be $16{\cdot}75/Re$. On the basis of computations using a number of different (Cartesian) grids and finite-difference methods this coefficient is estimated to be correct to within $\pm 0{\cdot}05$. Therefore f/f_0 for laminar flow was 1·047, where f_0 is the friction factor of the equivalent circular duct. Hence, using the equations given by Malak *et al.*, f/f_0 for turbulent flow is estimated to be 1·021. The measured value of this ratio is 0·976.

4.4. *Wall shear stresses*

The shear stresses on the walls of the test quadrant were found by Preston tube using the calibration proposed by Patel (1965), in the tabular form of Head & Vasanta Ram (1971). The results are shown in figures 3(*a*, *b*), normalized by the mean wall shear stress (as found by integration around the walls of the quadrant). Uncertainties on the wall shear stresses are estimated to be $\pm 0{\cdot}5\%$ on individual values and $\pm 2\%$ on the integrated mean value. The higher uncertainty on the integrated value is a consequence of an inadequate number of measurements in the corners of the duct where the stress varies rapidly.

The mean wall shear stress was found to be 2·394 N/m² by integration and 2·399 N/m² by calculation from the measured pressure gradient (at the nominal Reynolds number of 200000). In view of the uncertainty of the integrated value the closeness of these two figures is a coincidence.

As the sharp corners of the duct are approached the distribution of the wall shear stress shows the characteristic deviation from a steadily falling pattern caused by the secondary flows generated in the corners.

The measured distribution of wall shear stress both on the flat walls and on the rod surface are significantly more uniform than the distribution computed with secondary flows suppressed. Secondary flows have the effect of equalizing the wall shear stresses around the walls of the duct.

4.5. *Mean axial velocities*

A detailed measurement of the distribution of the mean axial velocities was done at a single Reynolds number of 200000. The measurements were made using a Pitot tube and were corrected for the effects of turbulence, velocity gradient, and wall proximity as suggested by Ower & Pankhurst (1966). It is estimated that the mean axial velocities are accurate to within $\pm 1\%$.

The measured contours of axial velocity normalized by the peak axial velocity are shown in figure 4(*a*). Distortions to the contours caused by secondary flows can be detected adjacent to the two corners. In comparison with the contours predicted with secondary flow suppressed the measured axial velocities are more uniform, a uniformity that extends from the core towards the gap and towards the flat side walls.

For a wide range of flows the velocity distribution normal to a wall can be expressed according to an inner law of the wall $U_+ = A \ln y_+ + B$ up to some maximum value

† The Kármán–Nikuradse expression is $f^{-\frac{1}{2}} = 4{\cdot}0 \log_{10} Ref^{\frac{1}{2}} - 0{\cdot}4$.

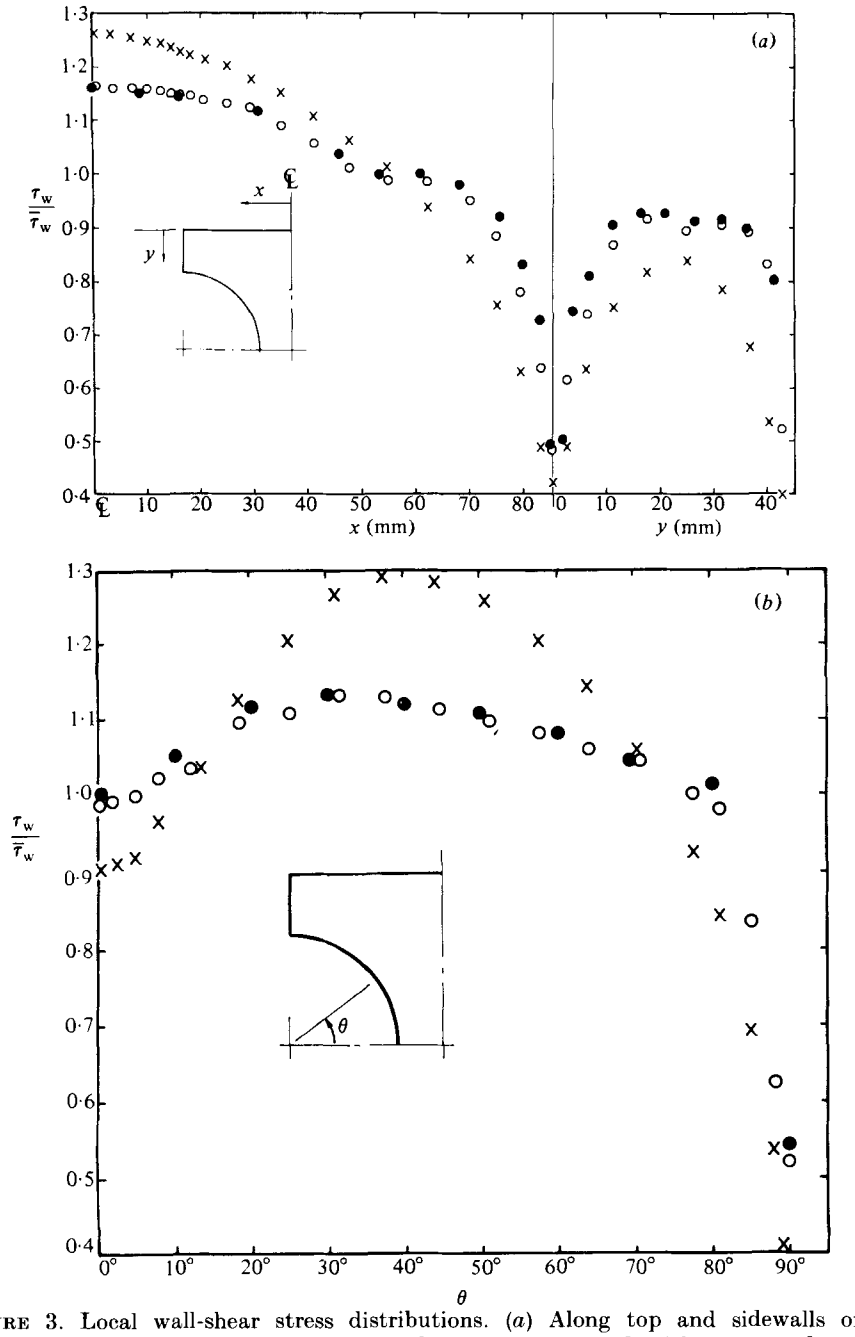

FIGURE 3. Local wall-shear stress distributions. (*a*) Along top and sidewalls of the duct ($Re = 200000$): ●, present experimental data; ×, computed without secondary flows; ○, computed with secondary flows. (*b*) Around rod surface ($Re = 200000$); ●, present experimental data; ×, computed without secondary flows; ○, computed with secondary flows.

of y_+. In the present case the mean axial velocities were normalized with the local friction velocity and the coefficients in the logarithmic law found for the traverses perpendicular to the top flat surface and for the radial traverses from the rod surface. Values of the coefficients A and B (as determined by a least-squares fit) for each traverse are given in table 2. Results for the traverses perpendicular to the flat surfaces

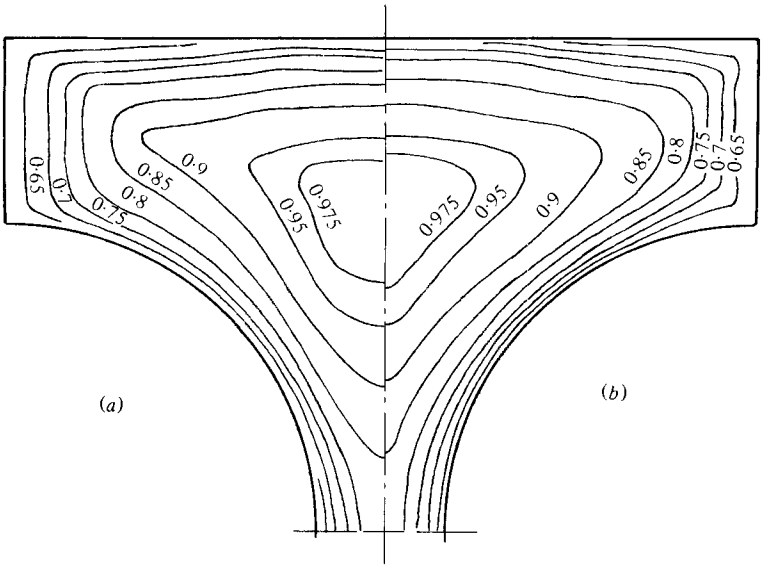

FIGURE 4. Contours of axial velocity (U/U_{max}) ($Re = 200000$): (*a*) from present experimental data; (*b*) computed (with secondary flows).

	Range y_+	A	B	Standard deviation of U_+ from LSF
Distance (mm) from vertical centre				
0	1600	2·562	3·919	0·409
15	1600	2·584	3·719	0·407
30	1600	2·608	3·918	0·243
45	1500	2·693	4·167	0·599
60	1500	2·671	4·219	0·289
75	700	2·670	4·320	0·383
Overall		2·638	4·008	0·251
Angular position from gap centre				
0°	1000	2·475	5·234	0·304
10°	1000	2·519	5·241	0·190
20°	1000	2·475	5·184	0·554
30°	1000	2·520	5·134	0·196
40°	1000	2·541	5·128	0·345
50°	1000	2·562	5·188	0·413
60°	1000	2·540	5·179	0·208
70°	1000	2·474	5·230	0·327
80°	1000	2·518	5·333	0·454
Overall		2·518	5·174	0·318

TABLE 2. Relations in form $U_+ = A \ln y_+ + B$ for each traverse (axial velocities normalized with local friction velocity)

all lay on a common line; similarly for all the radial traverses from the rod surfaces. However, there were differences between the two sets of results. For all traverses:

$$U_+ = 2{\cdot}638 \ln y_+ + 4{\cdot}008 \quad (S(U_+) = 0{\cdot}251), \text{ from the top flat surface}$$

$$U_+ = 2{\cdot}518 \ln y_+ + 5{\cdot}174 \quad (S(U_+) = 0{\cdot}318), \text{ from the rod surface}$$

where $S(U_+)$ is the standard deviation of the measured values of U_+ from the least-squares line. The equations apply for y_+ up to 1500, except in the corner regions, where the flow is influenced by the presence of the side wall.

4.6. *Reynolds stresses*

The Reynolds stresses were measured at a Reynolds number of 200000 using the rotated hot-wire technique; the extremely small secondary shear stress $-\rho\overline{vw}$ was not measured. Full details of the results are given in Seale (1981).

The effective cooling velocity U_e experienced by the wire was expressed as

$$U_e^2 = U(\sin^2\phi + F\cos^2\phi), \tag{9}$$

where U is the actual velocity, ϕ is the angle between the wire and the direction of U, and F is a direction sensitivity coefficient that accounts for the cooling effect of the velocity parallel to the hot wire. Kjellström (1974) recommended a value of 0·04 for F, and in the present work this value was also found to give the best agreement between the wall shear stress measured by the Preston tube and that found (after extrapolation to the wall) using the hot wire.

An analysis of the inaccuracies involved in the measurement of the Reynolds stresses (see appendix B) indicated that the three normal stresses and the shear stress $-\rho\overline{uv}$ are accurate to about $\pm 7\%$, whereas the transverse shear stress $-\rho\overline{uw}$ is probably not accurate to better than $\pm 17\%$. Repeated measurements, using different probes, of the axial shear stress $-\rho\overline{uw}$ showed a maximum variation of $0{\cdot}05\rho U_\tau^2$ and a typical variation of $0{\cdot}03\rho U_\tau^2$, where U_τ is the local friction velocity. Similar results were obtained for the normal stresses and for the transverse shear stress $-\rho\overline{uw}$. Since over most of the flow adjacent to the top flat surface the values of the transverse shear stress were of the order $0{\cdot}01\rho U_\tau^2$ consistent results were not achieved for this stress. Consequently it was not possible to analyse the results in terms of an effective eddy viscosity parallel to the top flat wall.

A further check on the accuracy of the Reynolds stresses was obtained by comparing the distribution of the axial shear stress, normalized using the local friction velocity, with a linear distribution between the wall and the point at which the gradient of the axial velocity normal to the wall is zero. A typical comparison is shown in figure 5. Although there is no reason to assume that this relationship is linear, gross departures from linearity would not be expected. Apart from the stresses close to the wall ($y/\hat{y} < 0{\cdot}1$) the measured distributions are fairly linear.

Quite close to the wall ($y_+ < 200$), however, a significant and consistent reduction in the axial shear stress below the straight line was observed. The source of this discrepancy could not be found despite repeated measurements and careful calibration procedures. Anomalous behaviour of the measured secondary velocities were also obtained. The region is too far from the wall ($y_+ = 100$–150) for the reduction in shear stresses to be caused either by the enhanced heat losses from the wire to the wall (important when $y_+ < 30$, Ota & Kostic 1972) or by the reduced turbulent stress component close to the wall. There were strong indications, however, that the source

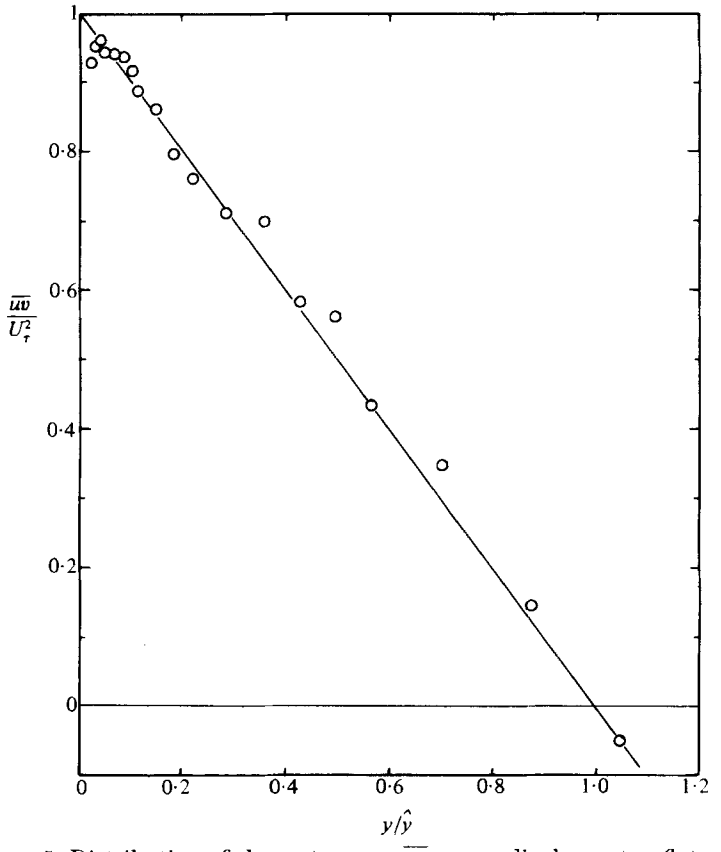

FIGURE 5. Distribution of shear stress $-\rho\overline{uv}$ perpendicular to top flat wall, 30 mm from vertical centreline (Re = 200000).

of the anomalous behaviour lay in differences in the velocity profile around the probe when it was very close to the wall as compared with the calibration jet.

A contour plot of the turbulence kinetic energy (normalized by the *mean* wall shear stress) is shown in figure 6(*a*). Although these contours were derived from a relatively coarse grid they clearly indicate convection of turbulent kinetic energy by secondary flows. The effect of the secondary flows generated in the corners is easily observed, but note also the way the contours in the core of the duct well removed from the corners, bulge in towards the centre.

Alshamani (1978, 1979) observed that axial (u), normal (radial) (v), and tangential (w) fluctuating velocity components show similar distributions in a number of pipe and two-dimensional channel flows. The velocity fluctuations are a minimum at the centreline, increase steadily as the wall is approached, and reach some maximum values close to the wall. Furthermore, the three fluctuating components vary in a similar way with Reynolds number.

In the region $0{\cdot}1 \leqslant y/\hat{y} \leqslant 1$ the fluctuating velocities (when normalized by the *local* wall-friction velocity) were shown to be related by simple linear equations, i.e.

$$\overline{v}_+ = A_1\,\overline{u}_+ + B_1, \quad \overline{w}_+ = A_2\,\overline{u}_+ + B_2,$$

where $\overline{v}_+ = v/U_\tau$, $\overline{w}_+ = w/U_\tau$, $\overline{u}_+ = u/U_\tau$ and $k_+ = k/U_\tau^2$. The curvature in the $k_+(\overline{u}_+)$ relationship implied by these equations was found to be small, and k_+ could also be

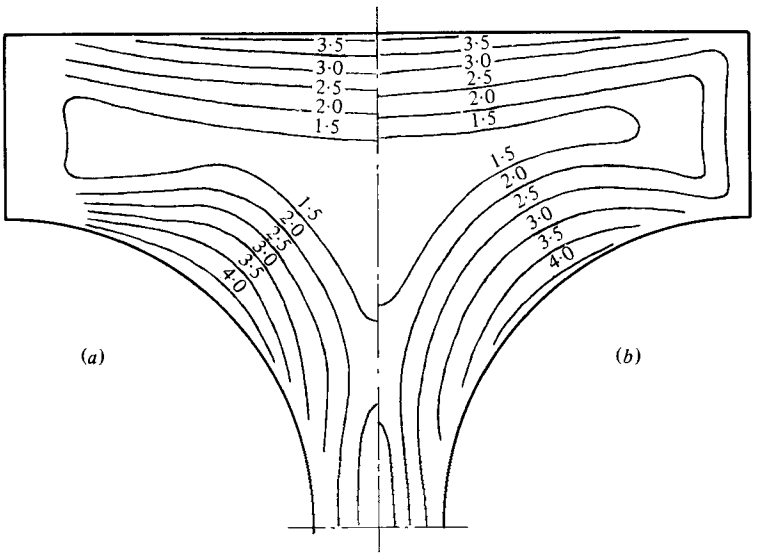

FIGURE 6. Contours of turbulence kinetic energy k/U_τ^2; $Re = 200000$: (*a*) from present experimental data; (*b*) computed (with secondary flows).

expressed as a linear function of $\bar{u}_+$, i.e. $k_+ = A_3\bar{u}_+ + B_3$. Alshamani examined a wide range of published experimental data and found that the coefficients of the linear equations varied by about $\pm 29\%$, although there was a much larger uncertainty on the coefficient B_2 for fully developed pipe flow. Nevertheless, in many experimental results there was a fair linear relationship between the fluctuating velocity components.

The Reynolds stresses in the current work have been plotted in the way suggested by Alshamani: typical results are shown in figure 7 (*a*) for all traverses normal to the top flat wall, and in figure 7 (*b*) for all the radial traverses from the rod surface. Despite the considerable scatter, especially of the fluctuating component normal to the wall ($\bar{v}_+$), the results appear to be capable of a linear representation. Moreover, within the level of uncertainty associated with the measurement of the turbulence quantities (about $\pm 10\%$) the results from all the traverses could be represented by single equations:

$$k_+ = 2{\cdot}40\bar{u}_+ - 1{\cdot}44, \quad \bar{w}_+ = 0{\cdot}587\bar{u}_+ + 0{\cdot}167, \quad \bar{v}_+ = 0{\cdot}303\bar{u}_+ + 0{\cdot}441.$$

These coefficients are different from those found by Alshamani.

The ability to express the turbulence quantities in this way emphasizes the essential similarity of the turbulence structure in the non-circular subchannel with the turbulence structure in a circular pipe. Similar results have been noted by Seale (1982) for the turbulence quantities in a triangular duct (Aly *et al.* 1978), in a square duct (Brundrett & Baines 1964), and in the subchannels of a simulated rod bundle (Rehme 1977).

4.7. *Secondary velocities*

The procedure given by Mojola (1974) was used to derive the secondary velocities from the response of the hot-wire anemometer. Details of the secondary velocities are given in Seale (1981); they are plotted in figure 8 (*a*) for velocities parallel to the top flat wall, and in figure 8 (*b*) for velocities perpendicular to the top flat wall. Note that the secondary velocities have been normalized by the mean friction velocity.

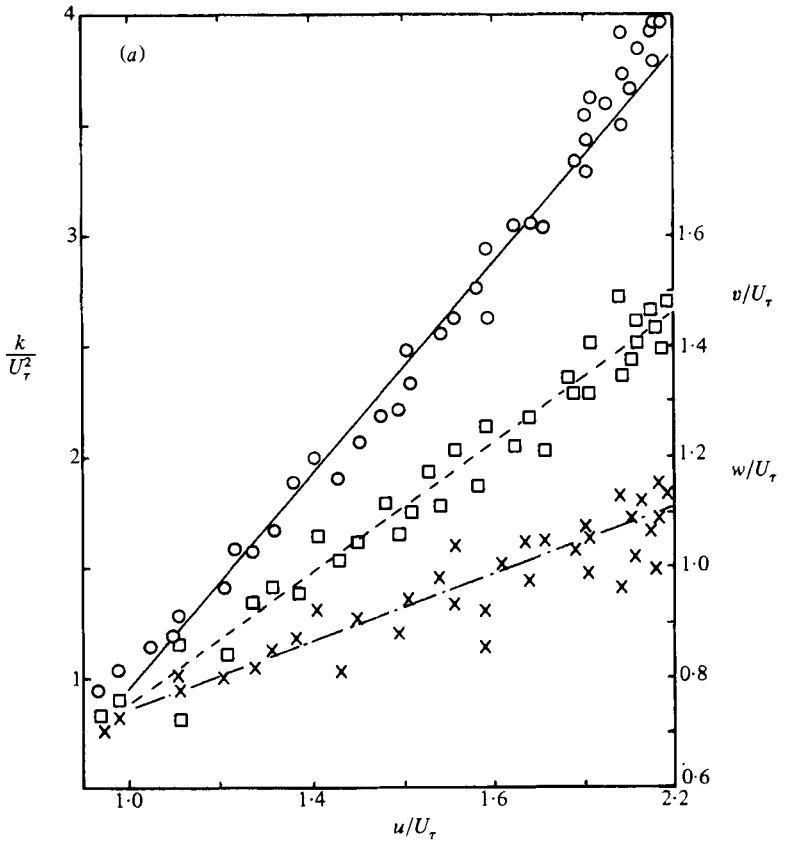

FIGURE 7. For caption see facing page.

The tiny secondary velocities were extremely difficult to measure, and the overall uncertainty of the secondary velocity W parallel to the top flat wall is estimated to be about $\pm 0{\cdot}06U_\tau$, where U_τ is the mean friction velocity (see appendix B). The results were repeatable to within about $\pm 0{\cdot}05U_\tau$.

The secondary velocity V perpendicular to the top flat surface reached a maximum value ($0{\cdot}35U_\tau$) very close to the surface ($y_+ < 200$). This unlikely behaviour is believed to be associated with the anomaly noted earlier in the measured shear stresses very close to the wall. Even away from the wall the velocity V continued to exhibit greater variations than the velocity W at the same point.

The accuracy of the measurements can be gauged by integrating the secondary velocities crossing any closed line within the symmetrical quadrant. The results of these calculations are given in table 3 and show a maximum imbalance in the flow crossing any vertical line to be $0{\cdot}047U_\tau$. Across any horizontal line, not near the top flat wall, the maximum imbalance was $0{\cdot}19U_\tau$ (partly a reflection of fewer measurements along horizontal lines). At $y_+ < 100$ this imbalance across a horizontal line was $1{\cdot}78U_\tau$, directed towards the wall. Note that the maximum secondary velocity was about $0{\cdot}35U_\tau$. The causes of the larger uncertainty on the secondary component V could not be found, neither could the persistent error close to the wall be eliminated.

The maximum secondary velocity parallel to the top flat wall is about 1·5 % of bulk velocity and occurs near the walls on the outward secondary flow from the corners

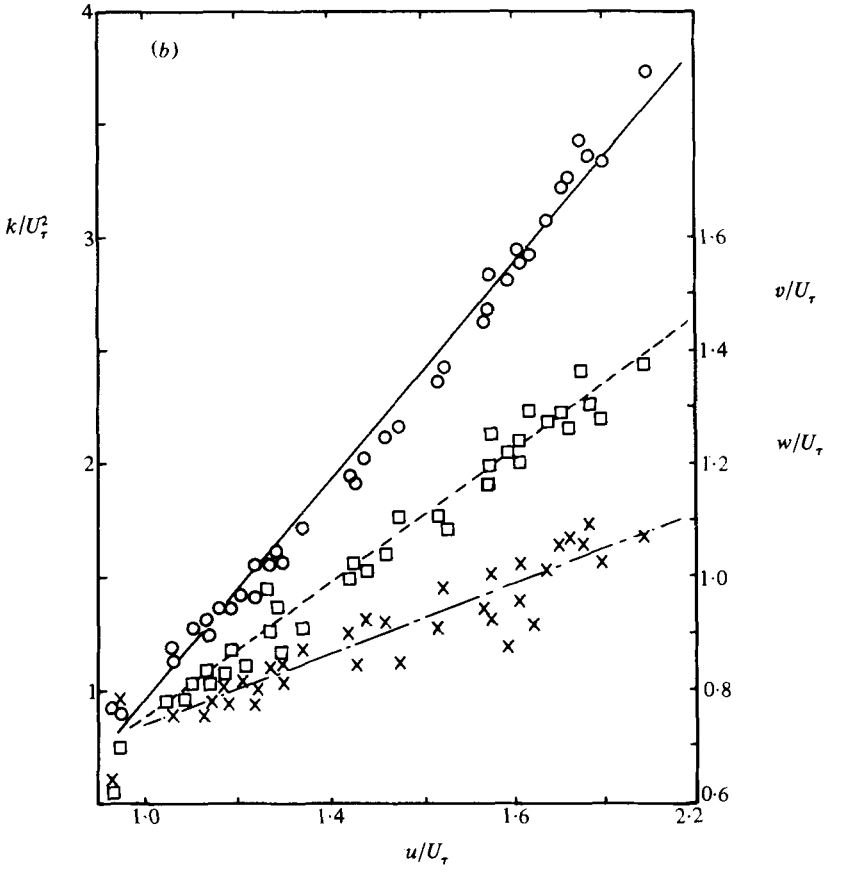

FIGURE 7. Turbulence kinetic energy and fluctuating velocities plotted against the axial fluctuating velocity: (*a*) perpendicular to top flat wall (selection of results from all traverses); (*b*) perpendicular to the rod surface (all angular positions). Results normalized with local friction velocity. ○, k/U_τ^2; □, w/U_τ; ×, v/U_τ; ———, $k_+ = 2{\cdot}40\bar{u}_+ - 1{\cdot}44$; - - -, $\bar{w}_+ = 0{\cdot}587\bar{u}_+ + 0{\cdot}167$; —·—·—, $\bar{v}_+ = 0{\cdot}303\bar{u}_+ + 0{\cdot}441$.

of the duct. The pattern and magnitude of the corner secondary flows are similar to those measured previously by Brundrett & Baines (1964) and Launder & Ying (1972). Apart from the secondary flows immediately in the corners there are two large rotating cells between the flat wall and the rod, and one cell in the gap region between the rod and the vertical axis of the duct. These cells move fluid from the core of the duct and direct it towards the flat sidewalls above the rods. The gap cell convects fluid down the centreline and returns it to the core along the walls of the rod surface.

5. Predicted results and discussion

5.1. *Axial velocities and turbulence kinetic energies*

A prime object of this work was to see whether use of the 'k–ϵ' turbulence model for the (isotropic) eddy viscosity together with a suitable model for the normal Reynolds stresses (to generate secondary flows) would allow the measured contours of axial velocity and turbulence kinetic energy to be reproduced. If secondary flows are excluded from the computations then it is not possible to obtain agreement with the measured results no matter how the empirical constants are optimized. In earlier work

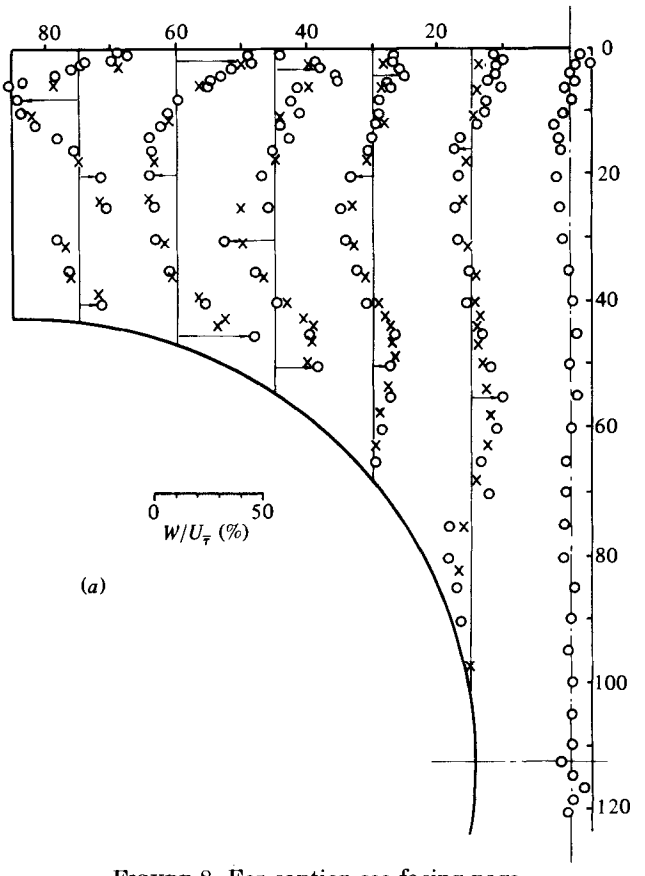

FIGURE 8. For caption see facing page.

Flow across a vertical line		Flow across a horizontal line	
Position of line from vertical axis (mm)	Net secondary velocity W/U_τ (%)	Position of line from top flat axis (mm)	Net secondary velocity V/U_τ (%)
0	−0·1	1	−176·7
15	0·67	5	18·7
30	0·53	20	−0·7
45	−3·3	35	13·8
60	−4·7	50	5·0
75	1·9	65	15·0

TABLE 3. Net flows crossing horizontal and vertical lines in symmetrical quadrant of duct

(Seale 1982), agreement could not be obtained using the Launder–Ying formulation for the difference in the normal stresses (equation (6)); hence an alternative approach had been necessary in which equation (7) for the source of axial vorticity was derived.

Use of this new model for the generation of secondary flows did allow the measured results to be reproduced. Comparisons between computations and experiment are shown in figure 6 for the turbulence kinetic energy, and in figure 4 for the axial velocity. Apart from the core region of the duct the results are satisfactory.

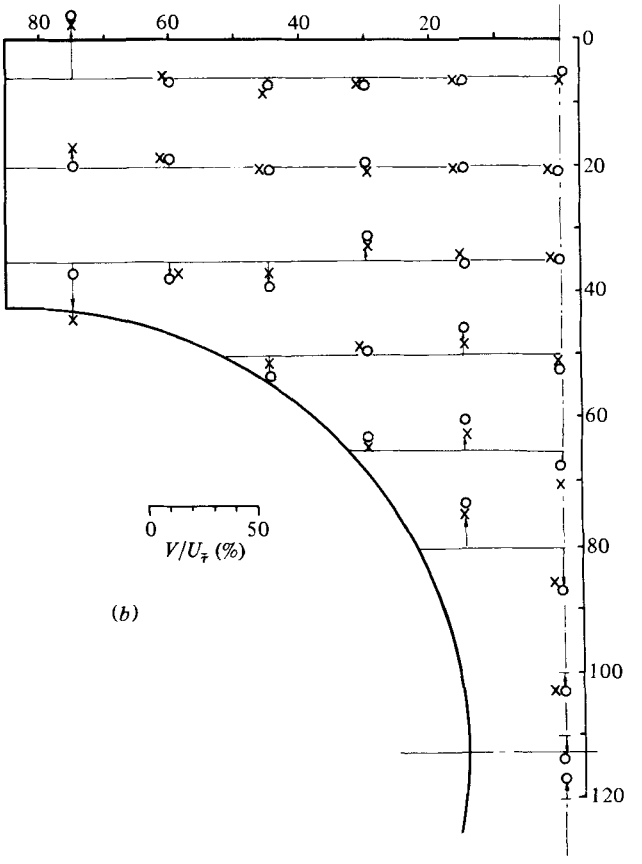

FIGURE 8. Secondary velocities normalized with mean friction velocity: (*a*) parallel to top flat surface (*W*); (*b*) perpendicular to top flat surface (*V*). ○, Present experimental results; ×, computed. (Distances in mm.)

5.2. *Secondary velocities*

In addition to the secondary flows in the sharp interior corners of the duct, the algebraic vorticity source yielded three main rotating secondary flow cells; these are shown in figure 9.

Comparisons between the measured and predicted secondary velocities are shown in figures 8(*a*,*b*); excellent agreement is obtained between the *patterns* of the flow cells. Velocities predicted and measured can be a factor of 2 different, but in general differ by about 30%.

5.3. *Wall shear stresses*

Wall shear stresses computed both with and without secondary flows are compared with those measured in figures 3(*a*,*b*). Suppression of the secondary flows increases the variation of the shear stress around the walls of the duct. Apart from near the sharp corners, where the finite difference grid was relatively coarse, close agreement with the measured shear-stress distribution is obtained when secondary flows are included in the computations.

5.4. *Friction factor*

Friction factors were calculated both with and without secondary flows over a range of Reynolds numbers and are shown in figure 2 in comparison with the experimental

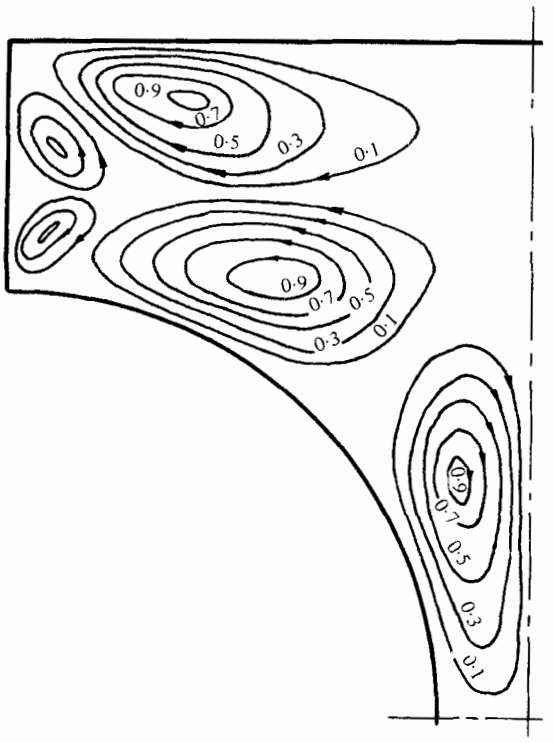

FIGURE 9. Computed distribution of stream function (ψ/ψ_{max}) in symmetrical quadrant of the duct. ($Re = 200000$).

results. The effect of including secondary flows in the calculations is to increase the friction factor by about 3·5%.

There is close agreement between the measured and predicted friction factors but there are differences in their variation with Reynolds number, viz

$$f = 0{\cdot}0376Re^{-0{\cdot}190} \quad \text{with secondary flows suppressed,}$$
$$f = 0{\cdot}0374Re^{-0{\cdot}187} \quad \text{with secondary flows included}$$

These should be compared with the experimental relationship

$$f = 0{\cdot}0475Re^{-0{\cdot}206}.$$

6. Conclusions

The following conclusions are for fully developed flow at a Reynolds number of 200000. The friction factors were measured over a range of Reynolds numbers from 82800 to 346700.

(i) The measured friction factors were represented by $f = 0{\cdot}0475Re^{-0{\cdot}206}$. This gives values 2% lower than predicted by the Kármán–Nikuradse correlation for friction factors in smooth circular pipes. According to the 'laminar-flow' method of Malak *et al.* (1975), the friction factor for this duct should be 2% greater than for the equivalent circular pipe.

(ii) The distribution of axial velocities normal to the walls and normalized with the local friction velocity can be expressed by the following inner laws of the wall for y_+ up to 1500 (except close to the corner regions), i.e. for all traverses normal to the flat wall

$$U_+ = 2{\cdot}638 \ln y_+ + 4{\cdot}008,$$

for all radial traverses from the rod surface

$$U_+ = 2{\cdot}518 \ln y_+ + 5{\cdot}174.$$

(iii) The distributions of the normal Reynolds stresses and the mean turbulence kinetic energy are similar to those observed in a number of pipe and two-dimensional channel flows, and for all points in the duct can be represented by the following equations:

$$k_+ = 2{\cdot}40\bar{u}_+ - 1{\cdot}44,$$
$$\bar{w}_+ = 0{\cdot}587\bar{u}_+ + 0{\cdot}167,$$
$$\bar{v}_+ = 0{\cdot}303\bar{u}_+ + 0{\cdot}441,$$

where the fluctuating velocities $\bar{u}_+$, $\bar{v}_+$, $\bar{w}_+$ have been normalized using the local friction velocity.

(iv) Secondary velocities have been measured to an accuracy of about $\pm 0{\cdot}06U_\tau$, and show a maximum value of 1·5 % of the bulk axial velocity.

(v) The 'k–ϵ' turbulence model for the isotropic eddy viscosity, together with the algebraic vorticity source for generating secondary velocities, enabled the calculation of axial velocities, mean turbulence kinetic energies and secondary velocities that were in satisfactory agreement with those measured.

All the experimental work reported here was done by Mr D. Mason, Senior Experimental Officer in the School of Mechanical Engineering, University of Bradford.

This paper is based on work performed under United Kingdom Atomic Energy Authority Contract WH 35554. Permission to publish is gratefully acknowledged.

Appendix A. Derivation of algebraic vorticity source

The algebraic expression (7) for the source of axial vorticity is developed in Seale (1982). For convenience a summary of the derivation is presented here.

For the prediction of secondary flows the source of axial vorticity has to be calculated (equation (5)), and this requires the specification of the distribution of the difference in the normal stresses $\bar{v}^2 - \bar{w}^2$. It was found, however, that existing measuring and prediction techniques did not allow this distribution to be specified with sufficient precision to obtain meaningful results. An alternative procedure is proposed in which the difference in the normal stresses is expressed in terms of the turbulence kinetic energy, i.e. from the results given in §4.6,

$$\bar{v}_+^2 - \bar{w}_+^2 = -0{\cdot}0441k_+^2 - 0{\cdot}0973k_+ + 0{\cdot}119.$$

This expression is substituted into (5) and reduced to the following approximate form:

$$S_\omega = 0{\cdot}045\rho U_\tau^2 \frac{\partial^2}{\partial y\,\partial z}(k_+^2 + 2k_+). \tag{A 1}$$

However, this equation remained extremely sensitive to the exact distribution of the turbulence kinetic energy, and it became necessary to generate a synthetic distribution of k_+ based on simple algebraic expressions. These expressions were derived after examining the flows in a number of ducts of non-circular cross-section, and were based on two assumptions: that the wall shear stress was uniform (this uniformity has been widely observed and is generally attributed to the presence of secondary flow) and that the distribution of k_+ along a normal to the wall was parabolic. Thus, after inspection of the distributions of k_+ measured in a square duct by Melling & Whitelaw

(1976), in a triangular duct by Aly *et al.* (1978), and in the present duct, the following expressions were derived:

$$k_+ = k_{i_+} + (k_{w_+} - k_{i_+})\,(1 - y/\hat{y}_{max})^2 \tag{A 2}$$

where $k_{i_+} = k_{c_+}(1 - 2{\cdot}4(1 - y/\hat{y}_{max})^2)$, $k_+ = k/U_\tau^2$, U_τ = friction velocity based on mean wall shear stress, k_{w_+} = value at the wall (taken as 4), k_{c_+} = value at centre of duct (taken as 1), y = normal distance from wall, $\hat{y}$ = normal distance from wall to surface of no shear, $\hat{y}_{max}$ = maximum value of $\hat{y}$ (for any given section). The surface of no shear is assumed to be coincident with the position of the maximum velocity on the normal from the wall. The algebraic expression for the source of axial vorticity was derived by combining (A 1) with (A 2), i.e.

$$S_\omega = 0{\cdot}864\,\frac{\bar{\tau}}{\hat{y}_{max}^2}\,Y_P\,Y_L\,Y_N\,\frac{d\hat{y}}{dz}, \tag{A 3}$$

where

$$Y_P = 1 - \hat{y}/\hat{y}_{max}; \quad Y_M = 1 - 2{\cdot}4\,Y_P^2, \; Y_L = 1 - y/\hat{y}_{max},$$

and

$$Y_N = \{1 + Y_M + (4 - Y_M)\,Y_L^2\} - \{(1 - Y_L^2)\,(4 - Y_M)\}.$$

In applying (A 3) it is necessary to refer each point in the flow to its nearest wall. The flow is then regarded as divided into a number of domains, each bounded by a wall and the surface of no shear. Note that Y_L is a normalized distance from the wall and varies from 1 at the wall to Y_P at the surface of no shear: the minimum value of Y_P is 0 in each flow domain. The direction of rotation of the vorticity is largely determined by the term $d\hat{y}/dz$, i.e. the rate at which the surface of no shear changes in the direction parallel to the wall.

Appendix B. Estimation of uncertainties in experimental data

The derivation of the five Reynolds stresses and the two components of the secondary velocity using the rotated hot-wire technique involved measurements from a hot-wire anemometer relocated five times to the same nominal position and the measurement of the mean axial velocity at the same position using a Pitot tube. In addition, the hot wire was calibrated before and after each traverse, and mean calibration constants derived. The analysis of errors was based on a sensitivity analysis done during the design of the experiment. Uncertainties have been estimated at a confidence level of at least 95 %. All uncertainties, regardless of type, have been combined by the 'root-sum-squares' method.

Reynolds stresses

For the derivation of the Reynolds stresses from the measurements, the following 'response' R_1 has to be constructed from the experimental results at each of the five hot-wire positions (Mojola 1974):

$$R_1 = \left(\frac{2E}{E^2 - E_0^2}\right)^2 \frac{\bar{e}^2}{n^2} = f\left\{\frac{\overline{u^2}}{U^2}, \frac{\overline{v^2}}{U^2}, \frac{\overline{w^2}}{U^2}, \frac{\overline{uv}}{U^2}, \frac{\overline{uw}}{U^2}\right\}, \tag{B 1}$$

where E and $(\overline{e^2})^{\frac{1}{2}}$ are respectively the d.c. and r.m.s. output from the anemometer, E_0 and n are the mean calibration constants, and U is the axial velocity measured by the Pitot tube. The uncertainties estimated for each measured quantity in R_1 are given in table 4. The uncertainty of $\pm 1{\cdot}6$ % in the measured response R_1 of the anemometer is incurred at each of the five hot-wire positions: its effect on the uncertainty of the Reynolds stresses (normalized by U^2) was estimated from the

	Uncertainty (±%)	Typical value
E (d.c. V)	0·03	5
$(\overline{e^2})^{\frac{1}{2}}$ (r.m.s. V)	0·05	0·05
$E^2-E_0^2$	0·5	18
U^2 (m/s)^2	1	700
mean calibration constants		
n	0·3	0·47
B	0·3	2·6
E_0^2	0·8	7
$R_1 = \left[\frac{2E}{E^2-E_0^2}\right]^2 \frac{\overline{e^2}}{n^2}$	1·6	

TABLE 4. Uncertainties in experimental measurements

	$\overline{u}^2$ (±%)	$\overline{v}^2$, $\overline{w}^2$, $\overline{uv}$ (±%)	$\overline{uw}$ (±%)
Relocation to 16 μm	0·2	0·7	2
Angle of wire (±0·1°)	0·4	1	3
Direction sensitivity F(±0·01)	0	3	3
Secondary velocities (±0·5% of U)	0	2	3
Response R_1	6	6	16
Overall uncertainty	6	7	17

TABLE 5. Constituents of the uncertainties in the measured Reynolds stresses

sensitivity analysis and shown in table 5. The sensitivity analysis was also used to estimate the size of the remaining sources of uncertainty: errors in relocating the probe and in measuring the angle between the wire and the duct axis for each of the five hot-wire positions, the assumption for the value of the direction sensitivity coefficient F (equation (9)), and the uncertainties in the measured secondary velocities. The results are shown in table 5. The overall uncertainty for each Reynolds stress varied with position from the walls, and the results, shown expressed as a percentage of the quantity being measured, are representative for most of the flow domain. However, the analysis showed that no stress could be measured with an absolute uncertainty less than $\pm 0{\cdot}02U_\tau^2$.

Secondary velocities

The secondary velocities were derived from the measurements of the anemometer using the response equations suggested by Mojola (1974). To illustrate the sources of uncertainty consider one of these equations reduced to the following simplified form:

$$\frac{W}{U_\infty} = \sqrt{2}\left\{\frac{R_A}{R_{A\infty}} - \frac{R_B}{R_{B\infty}}\right\}, \tag{B 2}$$

where $R = (E^2-E_0^2)^{1/n}$ can be regarded as the response of the anemometer to the mean velocity, subscripts A and B refer to measurements obtained with the hot wire held at two different angles to the flow, and subscript ∞ refers to measurements taken at a position in the core of the duct where the secondary velocities are believed to be zero.

Four major sources of uncertainty are associated with the use of (B 2): the precision of relocating the hot wire after rotation, drift in mean tunnel velocity during a traverse, calibration drift during a traverse, and the uncertainty in measuring the response R of the anemometer. The position of the hot wire was known to 16 μm. It was estimated that this would produce an uncertainty of $\pm 0{\cdot}05\,\%$ in U_∞ (mainly arising from the gradient of axial velocity). The mean tunnel velocity was constant to within $\pm 0{\cdot}05\,\%$ of U_∞. The uncertainty in obtaining the response R arose from the precision in measuring E ($\pm 0{\cdot}03\,\%$), and was estimated to be $\pm 0{\cdot}12\,\%$. The anemometer was calibrated before and after each traverse and a mean calibration obtained. The results were accepted if for a given voltage the velocities given by the two calibrations did not change by more than 1 %. It was found that if this condition was satisfied then the change in the response R would be less than $0{\cdot}25\,\%$, despite larger changes between the two calibrations in each of the individual calibration constants (see table 4). When combined to form the response R the directions of the changes in the individual constants were invariably such that they tended to cancel. The response R was formed using the mean calibration constants: uncertainty because of differences from the mean was therefore $\pm 0{\cdot}13\,\%$.

Combining these four major sources of uncertainty gives an uncertainty in R/R_∞ of $\pm 0{\cdot}18\,\%$. The secondary velocity is given by the difference between two such terms. Combining the uncertainties using the 'root–sum–square' method gives an overall uncertainty on V/U_∞ of about $\pm 0{\cdot}3\,\%$. Expressed in terms of the mean friction velocity this becomes $\pm 0{\cdot}06 U_\tau$.

REFERENCES

Alshamani, K. M. M. 1978 *A.I.A.A. J.* **16**, 859.

Alshamani, K. M. M. 1979 *Aero. J.* **83**, 159.

Aly, A. M. M., Trupp, A. C. & Gerrard, A. D. 1978 *J. Fluid Mech.* **85**, 57.

Bartzis, J. G. & Todreas, N. E. 1979 *Trans. A.S.M.E.* C: *J. Heat Transfer* **101**, 628.

Bearman, P. W. 1971 *DISA Info.* no. 11, p. 25.

Brundrett, E. & Baines, W. D. 1964 *J. Fluid Mech.* **19**, 375.

Carajilescov, P. & Todreas, N. E. 1976 *Trans. A.S.M.E.* C: *J. Heat Transfer* **98**, 262.

Gosman, A. D., Pun, W. M., Runchal, A. K., Spalding, D. B. & Wolfshtein, M. 1969 *Heat and Mass Transfer in Recirculating Flows.* Academic.

Gosman, A. D. & Rapley, C. W. 1980 *Recent Advances in Numerical Methods in Fluids.* Pineridge.

Hanjalic, K. & Launder, B. E. 1972 *J. Fluid Mech.* **52**, 609.

Head, M. R. & Vasanta Ram, V. 1971 *Aero. Q.* **22**, 295.

Hoagland, L. L. 1960 Ph.D. thesis, M.I.T.

Hooper, J. D. 1980 *Nucl. Engng Des.* **60**, 365.

Kacker, S. C. 1973 *J. Fluid Mech.* **57**, 583.

Kjellström, B. 1974 *AB Atomenergi Rep.* AE-487.

Launder, B. E. & Spalding, D. B. 1974 *Comp. Methods Appl. Mech. & Engng* **3**, 269.

Launder, B. E. & Ying, W. M. 1972 *J. Fluid Mech.* **54**, 289.

Launder, B. E. & Ying, W. M. 1973 *Proc. Inst. Mech. Engrs* **187**, 455.

Malak, J., Hejna, J. & Schmid, J. 1975 *Int. J. Heat Mass Transfer* **18**, 139.

Melling, A. & Whitelaw, J. H. 1976 *J. Fluid Mech.* **78**, 289.

Mojola, O. O. 1974 *DISA Info.* no. 16, p. 11.

Nijsing, R. & Eifler, W. 1970 *Des Deutschen Atomforums, Berlin.*

Ota, S. & Kostic, Z. 1972 *DISA Info.* no. 13, p. 29.

Ower, E. & Pankhurst, R. C. 1966 *The Measurement of Air Flow.* Pergamon.

PATANKAR, S. V. & SPALDING, D. B. 1970 *Heat and Mass Transfer in Boundary Layers*. Intertext.
PATEL, V. C. 1965 *J. Fluid Mech.* **23**, 185.
REHME, K. 1973 *Int. J. Heat Mass Transfer* **16**, 933.
REHME, K. 1977 *INR Rep.* KFK 2441 (English Transl. *UKAEA W.H. Transl.* no. 404).
REHME, K. 1978 *Nucl. Engng Des.* **45**, 311.
ROWE, D. S., JOHNSON, B. M. & KNUDSEN, J. G. 1974 *Int. J. Heat Mass Transfer* **17**, 407.
SEALE, W. J. 1977 Ph.D. thesis, University of Bradford.
SEALE, W. J. 1979 *Nucl. Engng Des.* **54**, 197.
SEALE, W. J. 1981 *University of Bradford Mech. Engng Rep.* no. 93.
SEALE, W. J. 1982 *J. Mech. Engng Sci.* (to be published).
TRUPP, A. C. & ALY, A. M. M. 1979 *Trans. A.S.M.E.* I: *J. Fluids Engng* **101**, 354.
TRUPP, A. C. & AZAD, R. S. 1975 *Nucl. Engng Des.* **32**, 47.